Available online at www.sciencedirect.com
SCIENCE DIRECT®
International Journal of Heat and Mass Transfer 47 (2004) 2523–2539
International Journal of HEAT and MASS TRANSFER
www.elsevier.com/locate/ijhmt

Numerical studies and experimental observations of whirling flames

A.Yu. Snegirev [a,*], J.A. Marsden [b], J. Francis [a], G.M. Makhviladze [a]

[a] Department of Built Environment, Centre for Research in Fire and Explosion Studies, University of Central Lancashire, Preston PR1 2HE, UK

[b] Greater Manchester County Fire Service, Fire Service Headquarters, 146 Bolton Road, Swinton, Manchester M27 8US, UK

Received 9 July 2003; received in revised form 5 February 2004

Abstract

The experimental observations and modelling of buoyant whirling flames in a room-size enclosure are presented. The periodic formation and destruction of whirling core, and the increase of the time-averaged burning rate have been observed in the experiments. To interpret the mechanism of development of buoyant whirling flames, the concepts and results of existing theory of rotating flows have been used, and the conditions necessary for flame rotation to occur have been identified. The CFD model is then discussed which is modified to represent the response of buoyant turbulent diffusion flame on the imposed circulation through decrease of turbulent mixing. The model is first applied to simulate unconfined flames above a round fuel source approximating the pool fire studied in the experiments. Elongation of whirling flames observed in published and our own experiments has been reproduced. The predicted flame characteristics (radius of whirling core, angular velocity, swirl number) dependence on the magnitude of the imposed external circulation was found in qualitative agreement with the simplified theoretical model of whirling flow. Also, the change of flame shape due to rotation resulted in reduced predicted radiative heat flux incident to fuel surface. This indicates the need of additional physical mechanisms to explain and predict the experimentally observed increase in burning rate when the rotation occurs. A possible mechanism, namely entrainment intensification of the air into the fuel rich region near the fuel surface, has been identified. Finally, the CFD model is applied to simulate the experimentally studied whirling flames in the enclosure. The simulation results recreated periodic precession, formation and destruction of the whirling flame as observed in the experiments. The period of oscillations was found to decrease if the fuel supply rate increases.

1. Introduction

Previous studies of structure and dynamics of buoyant turbulent diffusion flames have been mainly focused on the flames and plumes developing in the stagnant atmosphere (see a review in [1]), and, more rarely, exposed to cross-winds [2–4]. However, qualitatively different flame behaviour is possible when a *whirling* flame develops [5,6]. Buoyant whirling flames are usually much longer than those normally expected in ordinary fires. They may be potentially more destructive due to greater burning rate, increased radiative output, higher concentration of heat release in a small region of rotating core, and unexpected smoke movement. The effect of rotation on structure and behaviour of buoyant flames is not similar to that of swirling jet flames, and it has not yet been thoroughly studied. A better understanding is needed to allow techniques to be developed that will counter the possible threat presented, and it can affect the choice of required type of fire extinguishment. Also, the development and stability of whirling flames are of fundamental interest for refined modelling of coherent and self-organised flame behaviour.

The development of whirling flame is a result of an imposed circulating flow. Rotating flows and flames can

* Corresponding author. Tel.: +44-1772-893239; fax: +44-1772-892916.
E-mail address: asnegirev1@uclan.ac.uk (A.Yu. Snegirev).

0017-9310/$ - see front matter © 2004 Elsevier Ltd. All rights reserved.
doi:10.1016/j.ijheatmasstransfer.2004.02.002

Nomenclature

C_μ, $C_\mu^{\min}$, C_ω	model constants for turbulent viscosity
C_μ^*	rotation-modified model constant for turbulent viscosity
g	gravity acceleration
k	turbulence kinetic energy
$\dot{m}_{\text{fuel}}$	fuel supply rate per unit fuel surface area
p	pressure
$\dot{Q}$	total heat release in flame
r_0	vortex core radius
r, θ, z	polar cylindrical coordinates
R	pool/burner radius
R_c	local radius of streamline curvature of mean flow
Ri	Richardson number
S	swirl number
t	time
u, v, w	Cartesian velocity components
v_r, v_θ, v_z	radial, angular, and axial velocity components
$\vec{V}$	velocity vector
x, y, z	Cartesian coordinates
x_0, y_0	Cartesian coordinates of flow symmetry axis

Greek symbols

χ_C, χ_{CO}	soot and carbon monoxide generation efficiencies
ΔH_C, ΔH_C^*	net heat of combustion, net heat of incomplete combustion
ε	turbulence dissipation rate
Γ, Γ_0	circulation, external circulation
ν	kinematic viscosity
μ_T	turbulent viscosity
ρ, ρ_0	density, reference density
$\hat{\sigma}$	stress tensor
Ω	angular frequency
$\vec{\omega}$	vorticity vector

Subscripts

r, θ, z	polar cylindrical coordinates

be classified in terms of the following three characteristics: the ratio of flow momentum to buoyancy (buoyant or forced jet flows), the mechanism (buoyant or forced, external or internal circulating flow) that provides the circulation, and flow spatial scale.

Depending on their characteristic size, rotating flows can be regarded as very large, large, medium, and small. *Very large* buoyant rotating flows occur in oceans and the atmosphere [7,8]; in this case background weak external vorticity introduced by the Earth's rotation is concentrated into a whirling core of characteristic size about 10^5 m. In *large* buoyant whirls, such as those produced in oil, forest or city fires, the external circulation imposed due to wind-shear effects is supposed to be the primary source of the vorticity, which is then concentrated and amplified in the rising buoyant flow. Soma and Saito [9] provided categorisation and historical examples of large fire whirls. The height of the whirling core may range from hundreds of meters to tens of kilometres (10^2–10^4 m). Consistent studies of *medium* scale buoyant whirling flames with characteristic size of order of 1–10 m have not yet been reported. However, as shown in this work, such a flame may develop in room-size compartments due to the external circulation of asymmetrically incoming buoyant airflow through the openings. Finally, *small* scale buoyant whirling flames have been reproduced in laboratory conditions having dimensions of order of 0.1–1 m and driven by the externally imposed circulation of either buoyant [9–14] or forced (generated by rotating screen [5,6,15–17]) flows.

Important examples of *forced* rotating flows are *jet swirling flames*, which are intensively employed in industrial applications, in particular in combustion chambers and industrial furnaces, gasoline and diesel engines, gas turbines, utility boilers, etc. [6]. The swirling is used as a mean of controlling flame size, shape, stability, and combustion intensity. The swirling flows result from the enforced spiralling motion, and the swirl velocity component (azimuthal or angular velocity) is internally imparted by swirl vanes or by tangential entry into the chamber [6,18]. Due to its importance in industrial applications, jet swirling flows have been thoroughly studied. The structure of these flows was found to depend on the degree of swirl, which is characterised by the swirl number, S (the ratio of the axial fluxes of angular and axial momentum [6]). At high degree of swirl, the vortex core becomes unstable, it exhibits oscillatory behaviour and, if the swirl is further increased ($S > 0.6$ [6]), the vortex breakdown occurs. The recirculation zone develops, with the shape of oscillating bubble; this time-dependent coherent structure is referred as the precessing vortex core. As a result, the lateral spreading of the flow is *increased* and the decay of the axial velocity is facilitated. Accordingly, turbulent mixing and the reaction rate are *increased*, due to which the flame is *shortened*, compared to a non-swirling one.

Thus, in jet swirling flames, the swirling is imposed *internally* due to rotation of forced incoming flow of reactants. However, qualitatively different effect of rotation on turbulent mixing and flame length has been observed in flows and flames submerged into a rotating

flow environment, i.e. where the circulation is *externally* imposed. In this case (the example of forced flow is the flow in a rotating pipe [19]; buoyant whirling flames studied here also fall in this category), the intensity of turbulence has been shown to decrease due to rotation because of the stabilising effect of the centrifugal force.

Experimental studies of *buoyant flames* in a rotating flow environment were initiated by work [20], where the rotation of buoyant flame above an alcohol pool was induced by tangential airflow incoming into cylindrical chamber through vertical slits in its walls. The whirling flame development was observed, and, dissimilar to jet swirling flames, flame *elongation* occurred. More consistent measurements and observations together with simplified modelling were carried out by Emmons and Ying [5]. A cylindrical mesh rotating screen (3.0 m height, 2.2 m diameter) was used as a source of the external circulating flow imposed on the buoyant flame above the 0.1 m diameter acetone pool. The rotation of the screen produced circulation up to about 4 m^2/s. Significant (by a factor of 5, compared to a non-rotating case) flame elongation was obtained when the vortex core developed. The burning rate also substantially increased compared to that of a non-whirling fire. Flame elongation was attributed to decrease of turbulence intensity, air entrainment and its mixing with the fuel due to turbulence stabilising role of centrifugal forces. Similar conclusions were derived in [15–17], where jet flames with controlled fuel supply rate (burner fires) also surrounded by rotating screens were studied.

These experiments with a rotating screen are the examples of flames with *enforced* external circulation. External circulation may also be induced by asymmetrically incoming *buoyant* airflow, such as in an experimental enclosure with vertical gaps between the walls used in [10–14]. Different types of fuel (heptane, kerosene, ethanol, and wood) were burned in pools of 8–20 cm diameter. At some particular gap widths, flame rotation was observed. Similar to the earlier experiments, *decrease* in turbulent fluctuations, *increase* in flame length and its luminosity were clearly indicated. Although reference is made to an increase of mass burning rate, no quantitative results have been provided. In [11], the instability of the whirling flame was observed: if its height exceeded that of the walls, then the vortex core was destroyed.

Thus, the behaviour of *buoyant* whirling flames and plumes, is remarkably different compared to *forced* swirling jets. It has been established in the above mentioned experiments with buoyant whirling flames that the rotation decreases the turbulence in the rising core, thus inhibiting turbulent mixing at the core boundary and the air entrainment through it. As a result, dissimilar to forced swirling flows in industrial burners, rotation of buoyant flows causes flame lengthening, with no recirculating zone inside the core.

Theoretical studies of buoyant whirling flows have mainly been undertaken for environmental *flows without combustion*. Morton [7] discussed the different mechanisms of vorticity production and amplification, and he emphasised the role of ambient vorticity. Stretching of the vortex tubes in rising flows was identified as an important source of vorticity. The Rossby number, one of the governing criteria, was introduced and estimated for a range of whirling flows. A recent review of buoyancy driven circulation patterns, including plumes and thermals, is given in [8].

Available theoretical analysis of *buoyant rotating flames* is based on strict limitations of the integral model [5] and the inviscid flow assumption [21]. There have been only few attempts to carry out CFD modelling of whirling flames [11,13,22]. In these studies, radiative transfer was not modelled and the effect of flow rotation on turbulent fluctuations was not considered. Computations [22] have not reproduced the substantial lengthening of rotating flames observed in experiments [5].

Previous research of rotating flames is therefore insufficient for two reasons. First, experimental studies of medium (room-size) scale whirling fires have not yet been reported, although fire whirls have been observed in large-scale mass fires, and were also reproduced at small scale. Further experiments are required to fill this gap, i.e. to examine the possibility of whirling flame development and its behaviour in compartment fires, industrial and domestic. Second, further modelling efforts and computer simulations are needed to overcome limitations of currently available CFD models. Most importantly, radiative transfer should be considered, and the effect of flow rotation on turbulence should be accounted for.

In this work, experimental observations of medium (room-size) scale whirling fires are presented, demonstrating that whirling flames may develop in compartment fires. The periodic formation and destruction of whirling core, and the increase of the time-averaged burning rate are addressed. Basic concepts of rotating flows are then summarised illustrating the mechanism of development of buoyant whirling flame and conditions for flame rotation to occur. The CFD model is discussed which is modified to represent the response of buoyant turbulent diffusion flame on the imposed circulation through decrease of turbulent mixing. The model is consequently applied to simulate buoyant whirling flames in open space and in the enclosure representing that used in our experiments.

2. Experimental study of whirling fire

2.1. Experimental set-up and procedure

Medium scale fire whirls are studied experimentally at the Training Centre of Greater Manchester County

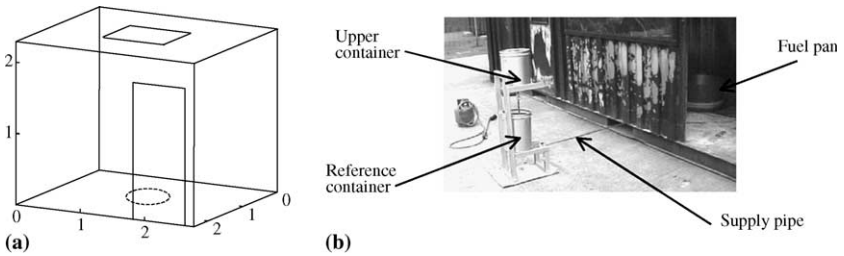

Fig. 1. Experimental set-up: (a) schematic view (measurements are in m); (b) fuel supply system.

Fire Service. Fire whirls are produced in a stand-alone compartment constructed of 5 mm thick corrugated steel with a hardwood floor. The schematic view of the compartment is shown in Fig. 1a. The compartment measurements are 2.77 m (front wall), 2.4 m (side wall) and 2.29 m (height). There is a doorway at the front wall having dimensions of 0.8 m width and 1.95 m height with its jamb at a distance of 0.135 m from the side wall. A ceiling vent measuring 0.8×0.9 m (longer side is along the front wall) is located centrally. The diameter of the fuel pan is 0.6 m, and the pan lip height is 0.3 m. The pan is located in the centre, i.e. directly underneath the vent opening. Commercially available diesel fuel (gas oil) was used. The fuel was ignited by industrial portable propane burner directed to the fuel surface. The burner flame provided sufficiently quick (5–10 s) heating of the liquid and initiation of self-sustained burning. The ignition process followed by flame development was recorded by video camera.

Two series of tests were carried out. In the first one, the initial mass (2–3 kg) of fuel was spilled into the pan, and the fuel available was completely burnt in the test; no liquid fuel was supplied in the pan during the experiment. In the second one, the system for continuous supply of liquid fuel into the pan was used. That allows the level of fuel surface in the pan to remain constant simultaneously measuring fuel flow rate. The fuel supply system consists of two fuel compartments and the supply pipe shown in Fig. 1b. The upper compartment is fitted with a controllable valve to vary the fuel flow. The reference compartment is used to measure fuel flow rate. This arrangement allows the amount of fuel used per unit time to be calculated therefore giving a time-averaged value for mass burning rate.

2.2. Experimental observations

Shortly after fuel ignition and flame spread over the entire fuel surface, the fire plume began to develop, and the upper hot smoky layer formed within the compartment, simultaneously exhausting through the ceiling vent and the upper part of the doorway. The maximum thickness of the layer was about 1 m. The plume then became unstable and began to rotate. While intensity of rotation reached its maximum, the upper layer gradually disappeared and eventually all the combustion products where expelled though the ceiling vent. The flame was significantly lengthened due to rotation, so that the flame was visible through the ceiling vent. After a short while the rotating flame became unsteady and then collapsed; it then behaved as an ordinary free-standing pool fire tilted by incoming airflow. This cycle then repeated itself and a rotating flame was again established. In the experiments with no liquid fuel supplied into the pan, the cycle repeated until all the fuel had been exhausted. The cycle period was about 10–15 s. Consequent stages of this oscillating process extracted from video recordings are presented in Fig. 2.

A series of experiments with continuous liquid fuel supply rate was undertaken to establish the mass burning rate for rotating and non-rotating cases. Rotating flames were obtained when the doorway was fully open. The non-rotating flames were achieved by a deflection of the incoming airflow towards the flame axis and were also obtained in the open atmosphere. In all cases, a 10 min pre-burn period was allowed to establish steady burning with the fuel level maintained constant, at a distance of 3–10 cm below the pan lip. Rotation of flame was found to result in observable (40–70%) increase in burning rate: from 0.017 to 0.027 kg/(m^2 s) in non-whirling to 0.029–0.039 kg/(m^2 s) in whirling fires.

Similar flame behaviour was observed in different weather conditions (temperature from 4 to 20 °C, external wind from 0 to 2 m/s). The flame behaviour was observed to be sensitive to the stronger external wind.

3. Basic concepts of rotating flows

3.1. Classification

To clarify the mechanism of development of whirling flame and conditions for flame rotation to occur, basic concepts of the existing theory of rotating flows [6,23] have been employed. A fluid flow rotating about its axis is convenient to be considered in cylindrical polar coordinates (r, θ, z) with corresponding radial, angular and axial (vertical) velocity components (v_r, v_θ, v_z). The

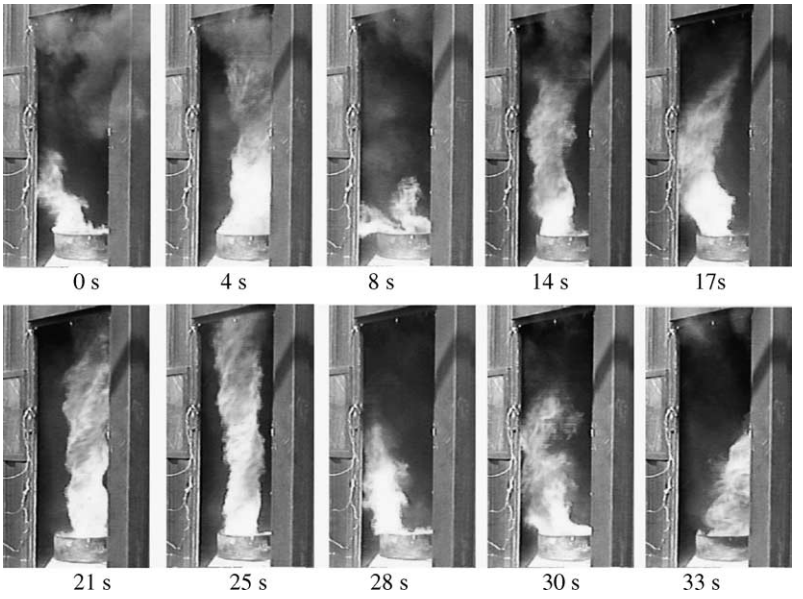

Fig. 2. Experimentally observed temporal evolution of whirling flame. Conventional time is set to zero for the first frame. Fully developed whirling flames occur at time moments of 4, 14, 24 and 34 c.

flow rotation is characterised by the vorticity vector, $\vec{\omega} = \nabla \times \vec{V}$, the angular frequency, $\Omega = v_\theta / r$, of rotation of a fluid particle about the axis, and the circulation, $\Gamma = \oint_l \vec{V}\,\mathrm{d}\vec{l}$, along a concentric path l, where $\mathrm{d}\vec{l}$ is the infinitesimal directed segment along l. To classify different types of rotating flows, consider an axisymmetric flow with no radial and axial velocity components. In such a flow, the angular (swirl) velocity, v_θ, is the only non-zero velocity component, and it depends on radius r. The vorticity vector has only one non-zero axial component, $\omega_z = \partial r v_\theta / r \partial r$. In the idealised (axisymmetric, steady state, laminar) flow, the momentum equation, $\mathrm{d}p/\mathrm{d}r = \rho v_\theta^2 / r$, represents balance between the centrifugal force and the pressure force.

Depending on the variation of the angular velocity with radius, three types of axisymmetric rotating flows (namely forced, free, and Rankine vortexes) are identified [6]. The *forced vortex* has non-zero constant vorticity and angular frequency. Its angular velocity and circulation increase with radius. The vorticity in the *free vortex* is zero (fluid particles follow a circular streamline without rotation about its own axis). Its angular velocity and frequency both tends to zero away from the axis, and its circulation is of constant value. These two types of flow are also different in terms of their stability. The outward radial fluid particle displacement (forced by centrifugal acceleration) is resisted by the pressure gradient, $\mathrm{d}p/\mathrm{d}r$, increasing with radius in the forced vortex. Alternatively, such a displacement is not compensated by the decreasing pressure gradient in the free vortex. As a result, fluctuations are stabilised in a forced vortex and destabilised in a free vortex [18].

The vortex that combines all these properties is the Rankine vortex, in which angular velocity increases with radius inside the vortex core and decreases outside it:

$$v_\theta \propto \frac{1}{r}\left(1 - \exp\left(-\frac{r^2}{r_0^2}\right)\right), \tag{1}$$

where r_0 can be regarded as the vortex core radius. Vortexes in rotating fluids are often of Rankine type. For example, this type of velocity distribution appears as a transient solution of vorticity diffusion away from an initial concentration on a vortex line [23, p. 204]. In that case, which is also called Lamb vortex (for example, see [24]), the radius of the vortex core increases in time as $r_0 = \sqrt{4\nu t}$, where ν is the kinematic viscosity. Also, a Rankine vortex forms in a rising rotating flow considered below in Section 3.2. Due to different response on fluid particles radial displacements, turbulent fluctuations are reduced (stabilised) in the internal (forced) part of the Rankine vortex and they are increased (destabilised) in its external (free vortex) part.

3.2. The vorticity equation. Sources of vorticity

Consider now a general buoyant flow with the momentum equation

$$\frac{\partial \vec{V}}{\partial t} + \left(\vec{V}\cdot\nabla\right)\vec{V} = -\frac{1}{\rho}\nabla p + \frac{1}{\rho}\nabla\hat{\sigma} + \frac{\rho - \rho_0}{\rho}\vec{g}, \tag{2}$$

where $\hat{\sigma}$ is the stress tensor that may include turbulent components if time averaged (mean) flow is considered, p is the dynamic pressure (difference between the total

pressure and the hydrostatic pressure in still ambient air). The evolution of vorticity in the flow is governed by the vorticity equation, which can be derived by taking curl of the momentum equation (2)

$$\frac{\partial\vec{\omega}}{\partial t}+\left(\vec{V}\cdot\nabla\right)\vec{\omega}=\underbrace{-\nabla\frac{1}{\rho}\times\nabla p}_{\text{baroclinic torque}}\underbrace{+\nabla\times\left(\frac{1}{\rho}\nabla\hat{\sigma}\right)}_{\text{viscous dissipation}}$$

$$\underbrace{-\nabla\frac{\rho_0}{\rho}\times\vec{g}}_{\text{buoyancy}}\underbrace{-\vec{\omega}(\nabla\cdot\vec{V})}_{\text{dilatation}}\underbrace{+(\vec{\omega}\cdot\nabla)\vec{V}}_{\text{stretching}}. \tag{3}$$

Analysis of this equation allows the vorticity sources in the flow to be identified, each corresponds to a particular term in right hand side of Eq. (3). In the flows studied, rotation about a vertical z-axis, i.e. in horizontal r–θ (or x–y) plane, is examined. The analysis can therefore be restricted by considering only the z-component of the vorticity vector. Written in cylindrical coordinates, the corresponding equation takes the form

$$\begin{aligned}&\frac{\partial\omega_z}{\partial t}+v_r\frac{\partial\omega_z}{\partial r}+v_\theta\frac{1}{r}\frac{\partial\omega_z}{\partial\theta}+v_z\frac{\partial\omega_z}{\partial z}\\&=\underbrace{+\frac{1}{r}\frac{\partial p}{\partial\theta}\frac{\partial}{\partial r}\frac{1}{\rho}-\frac{\partial p}{\partial r}\frac{1}{r}\frac{\partial}{\partial\theta}\frac{1}{\rho}}_{\text{baroclinic torque}}\underbrace{+\nu\left(\frac{1}{r}\frac{\partial}{\partial r}r\frac{\partial\omega_z}{\partial r}+\frac{1}{r^2}\frac{\partial^2\omega_z}{\partial\theta^2}+\frac{\partial^2\omega_z}{\partial z^2}\right)}_{\text{viscous dissipation}}\\&\underbrace{+0}_{\text{buoyancy}}\underbrace{-\omega_z\left(\frac{1}{r}\frac{\partial rv_r}{\partial r}+\frac{1}{r}\frac{\partial v_\theta}{\partial\theta}+\frac{\partial v_z}{\partial z}\right)}_{\text{dilatation}}\\&\underbrace{+\omega_r\frac{\partial v_z}{\partial r}+\omega_\theta\frac{1}{r}\frac{\partial v_z}{\partial\theta}+\underline{\underline{\omega_z\frac{\partial v_z}{\partial z}}}}_{\text{stretching}},\end{aligned} \tag{4}$$

where the viscous dissipation term is written for a constant viscosity flow, and ν is the kinematic viscosity. The very last (underlined) summand in the stretching term causes the amplification of non-zero vorticity, ω_z, in vertically accelerating flow in which $\partial v_z/\partial z>0$. In a buoyant flame and a plume, buoyancy force causes vertical acceleration of the flow inside the flame zone. That results in increase of ω_z provided the non-zero background vorticity is introduced. This is the explanation of development of a rotating core in a rising buoyant flow.

The term $\omega_z\partial v_z/\partial z$ becomes negative in the upper plume where axial velocity decreases with height. In this region the vortex tubes are not stretched but expanded, due to which the vorticity is decreased. Viscous and turbulent dissipation also results in decrease of vorticity, while the baroclinic torque and dilatation may change their sign in the flow.

3.3. Vorticity concentration in axisymmetric flow

A useful example of a simple flow, in which the vorticity is intensified due to stretching of the vortex tubes and balanced due to lateral spreading by viscous dissipation, is given in [23, p. 272]. The axisymmetric constant properties flow is considered for which the transport equation for ω_z takes the form (4) with the baroclinic and dilatation terms equal to zero. In the region $z\geqslant 0$, $r\geqslant 0$, $0\leqslant\theta<2\pi$ the solenoidal velocity field is assumed,

$$v_r=-\alpha r/2,\quad v_\theta=v_\theta(r),\quad v_z=\alpha z,\quad \alpha>0 \tag{5}$$

representing vertically accelerating rotating flow, which may be considered as a rough approximation of a rising whirling plume. Then Eq. (4) has a steady-state solution ω_z, which does not depend on θ and z:

$$\omega_z=\omega_{z\max}\exp\left(-\frac{r^2}{r_0^2}\right), \tag{6}$$

where

$$r_0=\sqrt{4\nu}/\alpha. \tag{7}$$

The angular velocity corresponding to (6) can be derived from $\omega_z=\partial rv_\theta/r\partial r$:

$$v_\theta=\frac{\omega_{z\max}r_0^2}{2r}\left(1-\exp\left(-\frac{r^2}{r_0^2}\right)\right). \tag{8}$$

It can be seen that the flow is in fact the Rankine vortex, Eq. (1). In this flow the concentration of vorticity into the vortex core is balanced by viscous dissipation, which results in three-dimensional flow also known as the Burgers vortex [24]. Typical streamlines of the flow are shown in Fig. 3.

The steady vorticity field, Eq. (6), is the distribution to which transient vorticity, $\omega_z(r,t)$, tends, as $t\to\infty$, if its initial distribution, $\omega_z(r,0)$, satisfies the condition

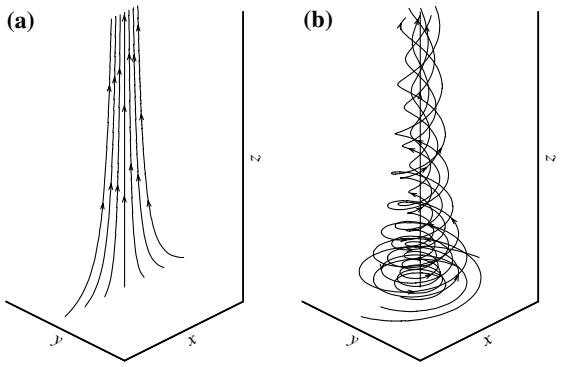

Fig. 3. Streamlines of the flow represented by Eqs. (5)–(8): (a) $\omega_{z\max}=0$; (b) $\omega_{z\max}$. Streamlines have the same origin points.

$$0 < \int_0^\infty \omega_z(r,0)2\pi r\,\mathrm{d}r < \infty. \tag{9}$$

It can be shown that for the flow considered the integral of the vorticity over a horizontal plane is invariant:

$$\frac{\mathrm{d}}{\mathrm{d}t}\int_0^\infty \omega_z(r,t)2\pi r\,\mathrm{d}r = 0, \tag{10}$$

where the integral is the circulation,

$$\Gamma_0 = \lim_{r\to\infty} 2\pi r v_\theta(r) \tag{11}$$

of the external flow. Therefore, the initial non-zero vorticity (and external circulation Γ_0) must be introduced for a steady rotating flow to develop; a spatial distribution of the initial vorticity may be arbitrary. As follows from Eqs. (8) and (11), the maximum vorticity $\omega_{z\max}$ in the steady vortex (6) is coupled with the external circulation:

$$\omega_{z\max} = \frac{\Gamma_0}{\pi r_0^2}. \tag{12}$$

According to Eqs. (5) and (7), the radius of the vortex core is

$$r_0 = \sqrt{\frac{4\nu}{\partial v_z/\partial z}}, \tag{13}$$

and therefore the maximum vorticity and angular velocity are

$$\omega_{z\max} = \frac{\Gamma_0}{\pi}\frac{\partial v_z/\partial z}{4\nu}, \quad v_{\theta\max} = 0.638\frac{\Gamma_0}{\pi}\sqrt{\frac{\partial v_z/\partial z}{4\nu}}. \tag{14}$$

Eqs. (14) show that the greater is the vertical flow acceleration and the smaller is the viscous (or turbulent) dissipation, the thinner and more intensive vortex core develops. Note, vortex radius (13) does not depend on the external circulation Γ_0. The overall degree of whirling can be characterised by the swirl number [6],

$$S = \frac{\int_0^\infty \rho v_z v_\theta r^2\,\mathrm{d}r}{R\int_0^\infty \rho v_x^2 r\,\mathrm{d}r}, \tag{15}$$

where (for the problem considered) R is the pool/burner radius. The swirl number presents the ratio of axial fluxes of angular and axial momentum (turbulent components and pressure term are neglected in (15)). It can be demonstrated for the flow considered, that the swirl number is proportional to the external circulation, i.e. $S \propto \Gamma_0$.

Thus, the existing theory of rotating flows reveals two necessary conditions for buoyant rotating flow to develop: (i) non-zero background vorticity (and external circulation) and (ii) vertical acceleration of the flow. The primary mechanism of vorticity concentration in the vortex core is the stretching of the vortex tube; the latter is balanced by viscous (and possibly turbulent) dissipation. When the above conditions are satisfied, the steady rotating flow has a radial velocity distribution similar to that of the Rankine vortex; the swirl number of the flow is proportional to the external circulation. The above mechanism works in buoyancy driven flows of a wide range of spatial scales, from small scale laboratory flows to circulating patterns in oceans and in the atmosphere. These results are reproduced by and used in the interpretation of the numerical simulations presented in this work, where the development of whirling buoyant turbulent diffusion flames are consequently simulated in the open space and in the enclosure.

4. Numerical modelling of whirling flames

4.1. Model and code

The 3D CFD model and code *Fire3D* earlier developed for predictions of open and enclosed buoyant turbulent diffusion flames [4,25,26] is used here in the simulations of buoyant whirling flames. The model is based on the density averaged continuity, specie conservation, momentum and energy equations for low Mach number turbulent multi-component flow (the components are fuel, O_2, CO_2, H_2O, N_2, CO, C) closed by use of k–ε turbulence model [27]. The conventional k–ε turbulence model does not take into account the effect of flow rotation. To make it capable in reproducing experimentally observed vortex stretching and augmentation in a rotating core, the model was modified as described later. A single-step global reaction of incomplete fuel oxidation that results in formation of carbon dioxide, water vapour, carbon monoxide and soot was used in this work. The soot and carbon monoxide generation efficiencies, χ_C and χ_{CO} (defined as the fractions of carbon atoms in the fuel converted to soot and carbon monoxide, respectively) are taken to be constant. The reaction rate was determined by the eddy break-up model [27]. The following parameters of gas fuel representing vaporised kerosene were used in the simulations: the chemical formula is $C_{14}H_{30}$, the enthalpy of formation is −387.5 kJ/mol (corresponds to net heat of combustion of $\Delta H_C = 44.1$ MJ/kg), the boiling temperature is 523 K, soot and carbon monoxide generation efficiencies are $\chi_C = 0.04$ and $\chi_{CO} = 0.007$ (net heat of incomplete combustion is $\Delta H_C^* = 41.6$ MJ/kg). The statistical (Monte Carlo) method is used to model thermal radiation transfer in gas–soot mixture, for which the effective absorption coefficient was obtained from total emissivity data obtained using weighted-sum-of-gray-gases model. The implementation of the method, the calculation of radiative properties of the gas–soot mixture, and the validation of the model against the measurements in buoyant turbulent non-rotating flames is fully described in [4,26], where the details of numerical methods can also be found.

4.2. Rotation modification for the turbulence model

In modelling of *jet* swirling flows, conventional isotropic eddy viscosity turbulence models, such as k–ε, fail to correctly represent a rotating flow field. For this kind of flow, several modifications were proposed and explored for the eddy viscosity turbulence models [18,28–31 among others]. Those modifications were through corrections in the source terms in the ε-equation or correction to the eddy viscosity,

$$\mu_{\mathrm{T}} = C_\mu \rho k^2/\varepsilon, \tag{16}$$

by expressing C_μ as a function of rotation. There is a little experience in numerical modelling of *buoyant* turbulent whirling flames. In simulations by [12] constant viscosity was assumed, and the performance of turbulence model was not addressed. In the work [22], where the experiment by Emmons and Ying [5] was modelled, the predicted flame lengthening due to imposed rotation was much less pronounced than that in the experiments, although the large eddy simulation technique was applied. In this work, where k–ε eddy viscosity model is employed, the approach previously used to improve the model performance in *jet* swirling flows (namely rotation dependent correction of C_μ) is applied in modelling of *buoyant* whirling flames. It will be shown that the conventional two-equation eddy viscosity turbulence model, after the ad hoc modification, allows the experimentally observed lengthening of rotating flames to be predicted.

Consider now the Rankine-type vortex distribution that combines solid-body and free vortex profiles as an approximation for a real vortex behaviour. As discussed above, the central forced vortex region $r < r_0$ (vortex core) exhibits flow field and turbulent characteristics, which are significantly different from those in surrounding irrotational vortex flow field. The traditional viewpoint is that the turbulence is stabilised by solid body rotation (i.e. inside the forced vortex core, where the turbulent fluctuations caused by centrifugal acceleration are resisted by the increasing pressure gradient) and destabilised by a free vortex profile [18]. To take this into account, the Richardson number, Ri, is introduced, that expresses the ratio of centrifugal force of the mean flow to a representative turbulent quantity. The conventional form of the Richardson number is [18]

$$Ri = \frac{\dfrac{v_\theta}{R_{\mathrm{c}}^2}\dfrac{\partial}{\partial R_{\mathrm{c}}} R_{\mathrm{c}} v_\theta}{\varepsilon^2/k^2}, \tag{17}$$

where R_{c} is the local radius of curvature of the streamline. The numerator in (17) is equal to $2\Omega^2$ in forced vortex core and tends to zero in the free vortex. Thus, in the core the Richardson number (17) is inversely proportional to the ratio squared of the period of rotation of the mean flow to the turbulent time scale, k/ε. There is however another way to define the Richardson number expressing the role of centrifugal acceleration of the mean flow explicitly:

$$Ri = \frac{\left(v_\theta^2/R_{\mathrm{c}}\right)^2}{\varepsilon^2/k}. \tag{18}$$

The latter relationship (where the Richardson number is set to the ratio squared of the centrifugal acceleration, $v_\theta^2/R_{\mathrm{c}}$, of the mean flow to the corresponding turbulent quantity, $\varepsilon/k^{1/2}$) was used in this work. The coefficient in the turbulent viscosity formula (16) was modified as follows:

$$C_\mu^* = (C_\mu - C_\mu^{\min})\exp(-C_\omega Ri^2) + C_\mu^{\min}, \tag{19}$$

where $C_\mu^{\min}$ and C_ω are the adjustable model constants. Note, the Richardson number corrections (either to the source terms in the dissipation equation or to the turbulent viscosity) have not been optimised for general rotating flows, and they can be case-dependent [18,32]. Also, the systematic experimental data on buoyant whirling flames, which can be used for the constant adjustment, are not available. However, it was concluded in [5] that due to flow rotation the turbulent plume mixing is reduced by an order of magnitude. We therefore assumed that $C_\mu^{\min}/C_\mu = 0.1$, where $C_\mu = 0.09$ is the conventional value. Reasonable predictions and relatively weak dependence of the simulation results on the numerical value of C_ω were obtained for $C_\omega < 0.01$. In the simulations performed, C_ω was set equal to 0.0012. Note, other than (19) modifications for C_μ were also proposed for swirling flows, for example one similar to that by Leschziner and Rodi [28]:

$$C_\mu^* = \frac{C_\mu}{1 + C_\omega Ri}. \tag{20}$$

Here we prefer to use Eq. (19) because, in contrast to Eq. (20), this dependence has an inflection point, $Ri^* = 1/\sqrt{2C_\omega}$, which separates regimes with negligible ($Ri < Ri^*$) and strong ($Ri > Ri^*$) effect of rotation on turbulence. For $C_\omega = 0.0012$ used in the simulations, $Ri^* = 20.4$.

To calculate the Richardson number, local radius of curvature and the angular velocity are required. In the problems addressed in this work, the radius of curvature should only account for flow rotation about the z axis. It was therefore calculated as [33] $R_{\mathrm{c}} = 1/\sqrt{x''^2 + y''^2}$, where $x'' = \partial^2 x/\partial s^2$, $y'' = \partial^2 y/\partial s^2$ are the derivatives of the fluid particle Eulerian coordinates taken in the streamwise direction, and s is the coordinate parallel to the streamline. Differentiation along the streamline yields

$$x'' = \frac{\partial}{\partial s}\left(\frac{\partial x}{\partial s}\right) = \frac{\partial}{\partial s}\left(\frac{\partial x}{\partial t}\frac{\mathrm{d}t}{\mathrm{d}s}\right) = \frac{\partial}{\partial s}\left(\frac{u}{q}\right) = \frac{1}{q^2}\left(\frac{\partial u}{\partial s}q - u\frac{\partial q}{\partial s}\right), \tag{21}$$

$$y'' = \frac{\partial}{\partial s}\left(\frac{\partial y}{\partial s}\right) = \frac{\partial}{\partial s}\left(\frac{\partial y}{\partial t}\frac{\mathrm{d}t}{\mathrm{d}s}\right) = \frac{\partial}{\partial s}\left(\frac{v}{q}\right) = \frac{1}{q^2}\left(\frac{\partial v}{\partial s}q - v\frac{\partial q}{\partial s}\right), \quad (22)$$

where $q = \mathrm{d}s/\mathrm{d}t = \sqrt{u^2+v^2}$, since only rotation in x–y plane, i.e. about z-axis, is considered. In the above equations,

$$\frac{\partial q}{\partial s} = \left(\frac{\vec{q}}{q}\cdot\nabla\right)q = \frac{1}{q}\left(u\frac{\partial q}{\partial x} + v\frac{\partial q}{\partial y}\right),$$
$$\frac{\partial u}{\partial s} = \left(\frac{\vec{q}}{q}\cdot\nabla\right)u = \frac{1}{q}\left(u\frac{\partial u}{\partial x} + v\frac{\partial u}{\partial y}\right),$$
$$\frac{\partial v}{\partial s} = \left(\frac{\vec{q}}{q}\cdot\nabla\right)v = \frac{1}{q}\left(u\frac{\partial v}{\partial x} + v\frac{\partial v}{\partial y}\right), \quad (23)$$

where $\vec{q} = u\vec{\mathbf{i}} + v\vec{\mathbf{j}}$. For a fluid particle that has coordinates (x, y, z), the centre of rotation in the horizontal plane was found as $x_c = x + x''R_c^2$, $y_c = y + y''R_c^2$. Radial and angular components of the velocity vector were then obtained from $v_r = u(x-x_c)/R_c + v(y-y_c)/R_c$, $v_\theta = -u(y-y_c)/R_c + v(x-x_c)/R_c$. Use of the modified coefficient C_μ^* (19) for the turbulent viscosity calculation provided significant improvement in the model capability to predict elongation of whirling flames.

4.3. Simulations of open whirling flames

Simulations were conducted of unconfined whirling flames above a fuel source of 0.6 m diameter centrally located at floor level (representing that used in our experiments). The flames were modelled in computational domain $0 < x < x_{\max}$, $0 < y < y_{\max}$, $0 < z < z_{\max}$ with $x_{\max} = y_{\max} = 2.4$ m, $z_{\max} = 3.29$ m. The non-uniform rectangular computational mesh consisted of a total of 102 400 control volumes ($40\times40\times64$ grid nodes). The grid nodes were concentrated in the flame zone to better resolve high gradients of the parameters. The fuel surface was spanned by 264 grid nodes. Minimum cell sizes were of $0.0375\times0.0375\times0.03$ m.

The externally imposed circulation was modelled through boundary conditions posed on the velocity components tangential to the vertical boundaries of the computational domain. These velocity profiles were chosen to represent a free (potential) vortex:

$$u(x) = -\frac{\Gamma_0}{2\pi}\frac{y-y_0}{(x-x_0)^2+(y-y_0)^2}, \quad y = 0, y_{\max},$$
$$v(y) = \frac{\Gamma_0}{2\pi}\frac{x-x_0}{(x-x_0)^2+(y-y_0)^2}, \quad x = 0, x_{\max}, \quad (24)$$

where x_0, y_0 are the coordinates of the flow symmetry axis (half of the horizontal size each), $\Gamma_0 = 2\pi x_0 u_{\max}$ is the external circulation, and $u_{\max}$ is the maximum tangential velocity at the boundary.

The effect of the external circulation on flames with different heat release rate was numerically studied. The fuel supply rate was varied from 0.010 to 0.040 kg/(m^2 s), which covers time-averaged burning rates measured in our experiments.

The steady state mean temperature fields and the flow streamlines for the flame with $\dot{m}_{\mathrm{fuel}} = 0.040$ kg/(m^2 s), which correspond to heat release rate of 516 kW, are shown in Fig. 4. Unconfined free-standing non-rotating flame ($u_{\max} = 0$ m/s, $\Gamma_0 = 0$ m^2/s), and the flames with relatively weak ($u_{\max} = 0.2$ m/s, $\Gamma_0 = 1.45$ m^2/s) and strong ($u_{\max} = 0.6$ m/s, $\Gamma_0 = 4.35$ m^2/s) imposed external circulation are presented. Clearly, the external circulation significantly affects the predicted flame shape and length. Similar to earlier reported measurements [5,6,11] and our observations (presented in Section 2), rotation may cause significant flame lengthening (Fig. 4b). However, the model also predicts flame shortening if the external circulation is greater than some particular value (Fig. 4c).

The turbulence model used in the calculations is of crucial importance for modelling flame lengthening due to rotation. The comparison of predictions for the axial temperature profiles given in Fig. 5 shows, that the standard version of k–ε model yields only minor increase in the flame length compared to the non-rotating case, while the modified model predicts the much longer rotating flame.

Figs. 6 and 7 show the effect of rotation on flame internal structure. In particular, Fig. 6 demonstrates that the vortex developed is of Rankine-type. The magnitude of the angular velocity is proportional to the external circulation (which is in accordance with the approximate theory, see (14)); it also depends on the flame heat release rate. In agreement with (13), radius of the vortex core is not affected by the magnitude of external circulation. Axial profiles of mean temperature and velocity are given in Fig. 7. It can be seen, for flames with relatively low heat release rate (for example, $\dot{m}_{\mathrm{fuel}} = 0.020$ kg/(m^2 s), $\dot{Q} = 258$ kW), the external circulation may cause a decrease in flame length, while rotating flames with greater heat release (see $\dot{m}_{\mathrm{fuel}} = 0.040$ kg/(m^2 s), $\dot{Q} = 516$ kW) are significantly longer than their non-rotating counterparts. This can be explained based on the results given in Section 3. Indeed, it has been demonstrated that the externally imparted vorticity is augmented by rising *accelerating* flow due to stretching of the vortex tube, while the vorticity in *decelerating* flow decays due to vortex tube expansion. The accelerating part of the flow is obviously greater for flames with higher heat release rate. As the vorticity is augmented, the increase of speed of rotation causes decrease of turbulent mixing of fuel with the air entrained, which is modelled through turbulent viscosity, Eq. (16), corrected using Eq. (19). Less intensive mixing of the reactants requires greater flame surface and,

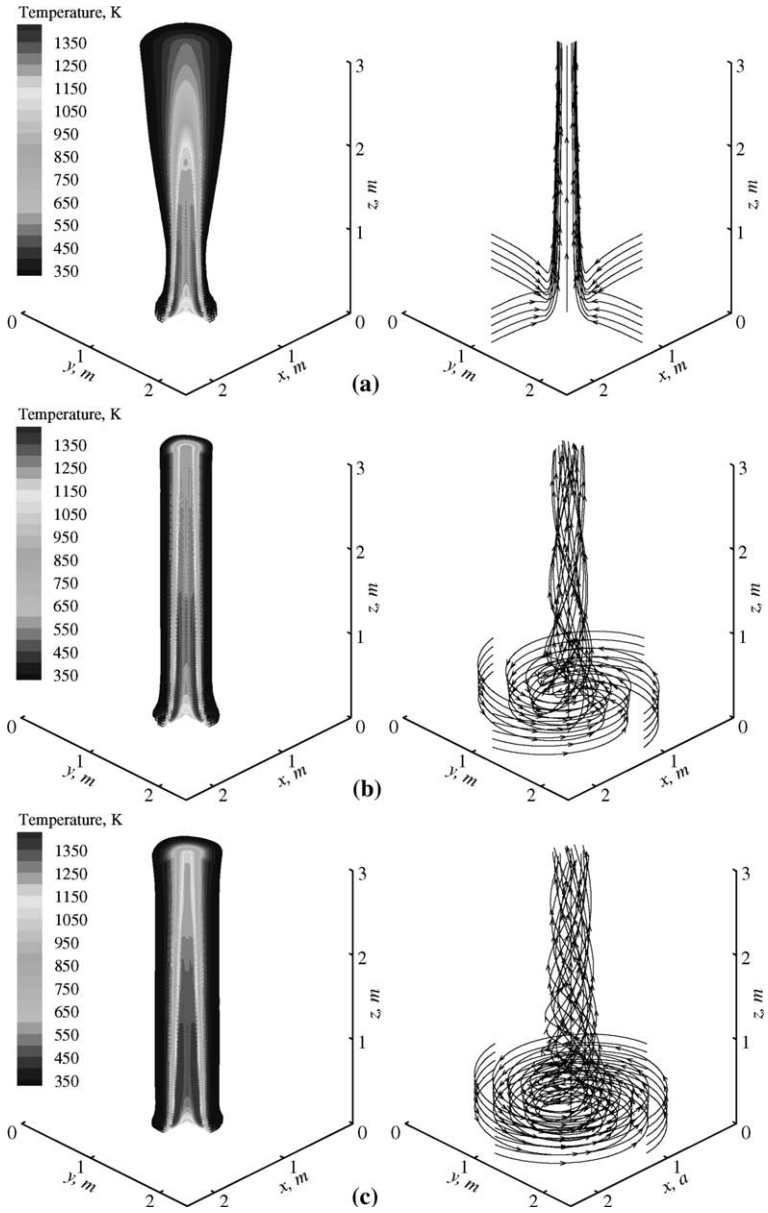

Fig. 4. Steady-state mean temperature fields (left) and mean-flow streamlines (right) in 516 kW flame: (a) Γ_0 m^2/s; (b) $\Gamma_0 = 1.45$ m^2/s; (c) $\Gamma_0 = 4.35$ m^2/s.

consequently, greater flame length. Opposite effect is obtained in the upper decelerating part of the plume.

As expected from consideration of a simple rotating flow (Section 3.3), the swirl number S, Eq. (15), obtained in the simulations is proportional to the imposed circulation, Γ_0 (see Fig. 8). When the swirl number exceeded 0.6, flame shortening indicated in Fig. 4c was predicted. Furthermore, flame with low heat release rate (such as 126 kW flame) became unstable, and the steady state was not reached. Note, behaviour of jet swirling flows also exhibits qualitative changes at high degrees of swirl ($S > 0.6$ [6]).

Fig. 9 compares the radiative heat fluxes (obtained by Monte Carlo method) emitted by the flames and calculated at the distance of 1.2 m from the flame axis. Since the rotating flames are normally thinner than non-rotating ones with the same heat release rate, while their maximum temperatures are approximately the same, the local radiative heat fluxes are reduced compared to non-rotating case. The change in flame shape also results in

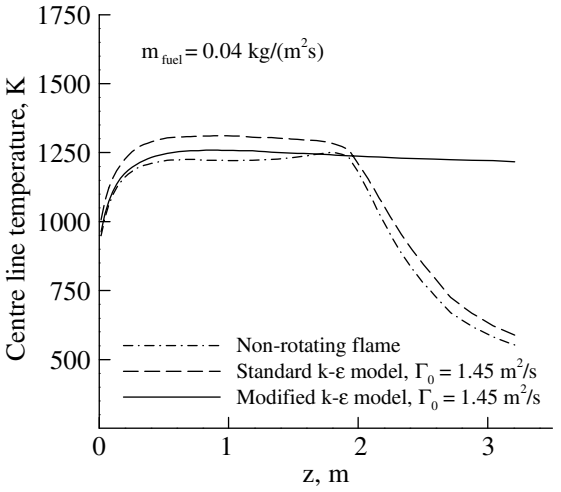

Fig. 5. The effect of turbulence modelling on the predicted flame centreline temperature.

some decrease of radiative heat flux incident to the fuel surface. It can therefore be concluded that rotation of the flow in the vortex core is not sufficient to provide the experimentally observed increase in burning rate in whirling flames above evaporating pools. However, the flow rotation intensifies the entrainment of the air into the fuel rich region *near the fuel surface*, which may intensify mixing of the reactants in this area, thus providing greater reaction rates, temperature, radiation emission, and evaporation rate. These phenomena may be a possible mechanism that causes the observed increase of burning rate due to rotation, and this mechanism has to be specially considered.

4.4. Simulations of whirling flames in enclosure

The experimental enclosure (see Section 1) is considered. The computational domain used in the simulations was expanded beyond the enclosure, having the dimensions of $3.4\times2.77\times3.29$ m. Non-uniform rectangular computational mesh consisted of 122880 control volumes ($48\times40\times64$ grid nodes). The mesh inside the enclosure was the same as that used for unconfined flames. Whirling flame was modelled with a constant prescribed fuel supply rate, which was varied from 0.010 to 0.040 kg/(m^2 s), the range covering time-averaged burning rates measured in our experiments. Fig. 10

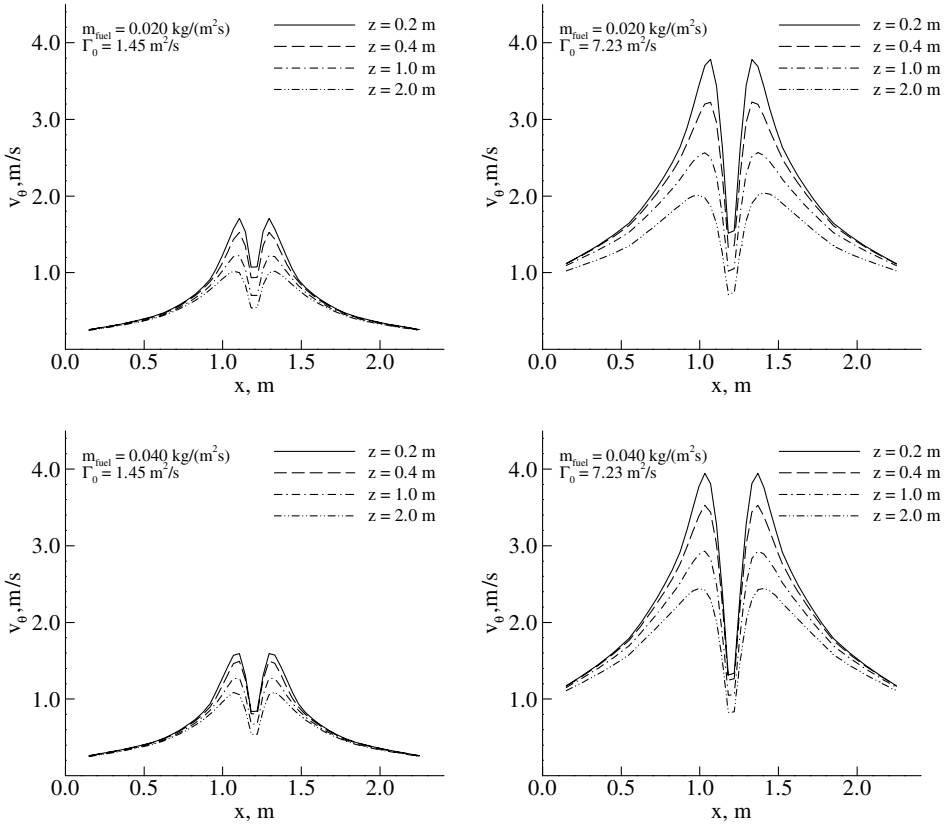

Fig. 6. Radial profiles of angular velocity.

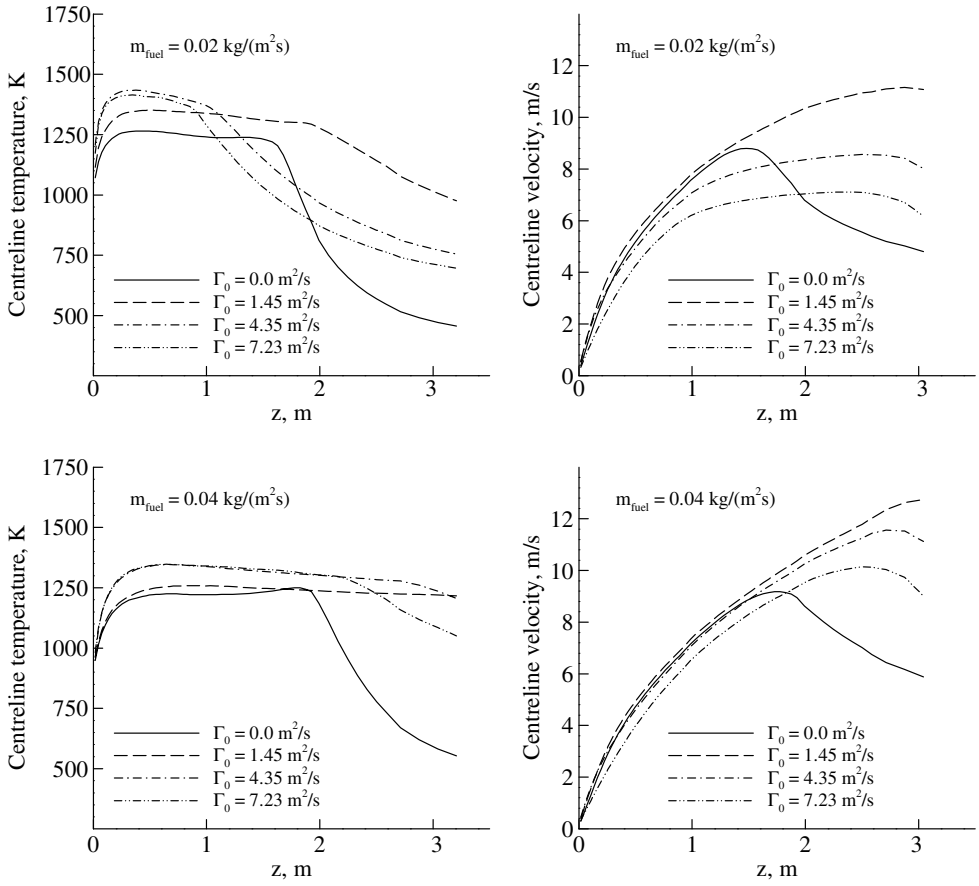

Fig. 7. Axial profiles of mean temperature and velocity.

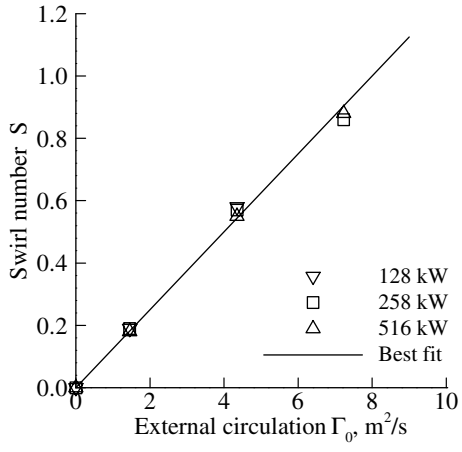

Fig. 8. Swirl number of rotating flows versus external circulation.

demonstrates a representative temperature-velocity field with the flame zone, incoming airflow, hot layer, and the outgoing flows leaving the compartment through the ceiling vent and the doorway. A time moment is shown, when straight rotating flame is exhausting through the ceiling vent.

The main finding from numerical simulations of the enclosed flames was their intrinsically transient behaviour and unsteadiness. Although the predicted mean temperature, velocity and all the other fields in unconfined flames of the same calorific power reached steady state, the enclosed flames appeared to be unsteady. The unsteadiness manifested itself through the precession of the flame and the periodic formation and destruction of the whirling high-temperature core. As discussed above, this phenomenon has been also observed in our experimental compartment.

The periodicity of the process is demonstrated in Fig. 11, where the maximum value of ω_z is shown as a function of time for three flames with different fuel supply rate. It can be concluded that the period decreases as the fuel supply rate increases. Therefore, more volatile combustibles are expected to produce a higher frequency of the process.

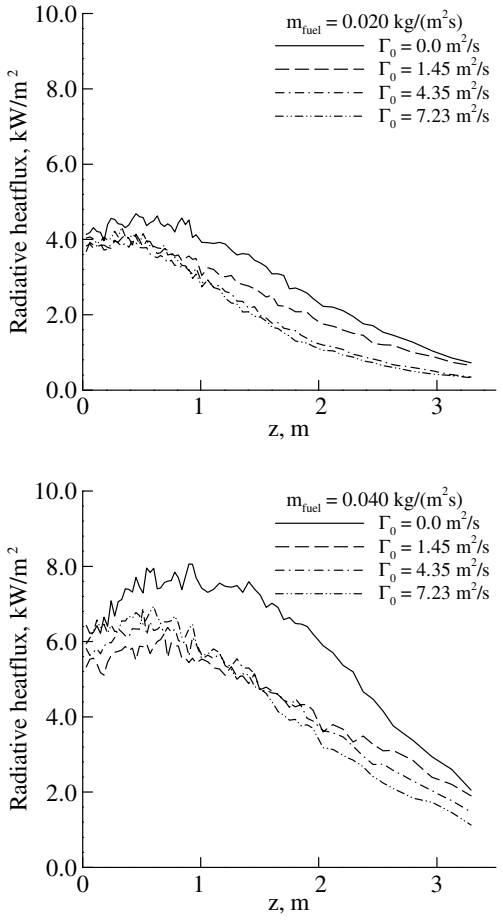

Fig. 9. Radiative heat fluxes at the distance of 1.2 m from the flame axis.

Frame by frame analysis of the predicted flame development has been performed, and different stages have been identified as shown by sequence of frames taken from video against temperature and vorticity fields with mean flow streamlines (see Fig. 12). When flame is deflected towards the corner near the front wall, no organised rotation occurs (Fig. 12a). Later on, the flame zone is driven by circulating incoming airflow towards the front wall and consequently to the doorway, when the vorticity slowly concentrates around the flame zone (Fig. 12b). Then the vortex core forms, the flame lengthens which results in formation of straight, long, relatively thin, and rapidly rotating flame (Fig. 12c and d). The flame and the vortex core coincide at this stage, duration of which appears to be very short. The air inflow displaces the upper part of the flame and the entire vortex core towards the rear corner (Fig. 12e). Since the vortex core and the flame no longer coincide, rotation no longer reduces turbulent mixing, and the flame shortens. Further downstream displacement of the vortex core (Fig. 12e) leaves it without a source of vorticity (which is due to vortex stretching in accelerating flow, see above), because of shorter length of the accelerating flow. Also, the upper part of the vortex tube is chopped off, because the tube is no longer directed towards the ceiling vent. Due to that, the vortex tube finally dissipates, and the non-rotating flame temporarily stabilises deflected to the left wall (Fig. 12f). Then the whole cycle repeats.

The average period between the formations of straight whirling flame determined from the simulations varied from 17 s for $\dot{m}_{\text{fuel}} = 0.020$ kg/(m^2 s) to 12 s for $\dot{m}_{\text{fuel}} = 0.040$ kg/(m^2 s), which is similar to the average period observed in our experiments (about 10–15 s).

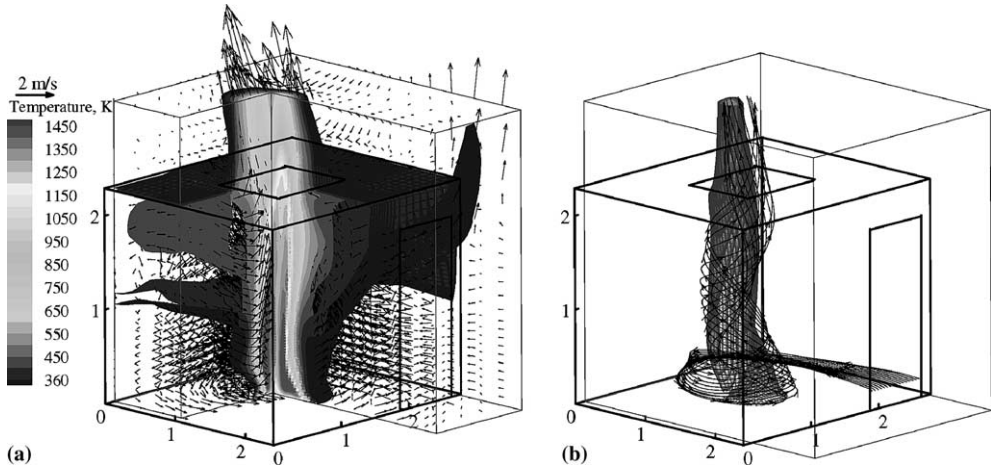

Fig. 10. The predicted straight rotating flame exhausting through the ceiling vent: (a) mean temperature and velocity fields; (b) mean-flow streamlines and 700 K temperature surface.

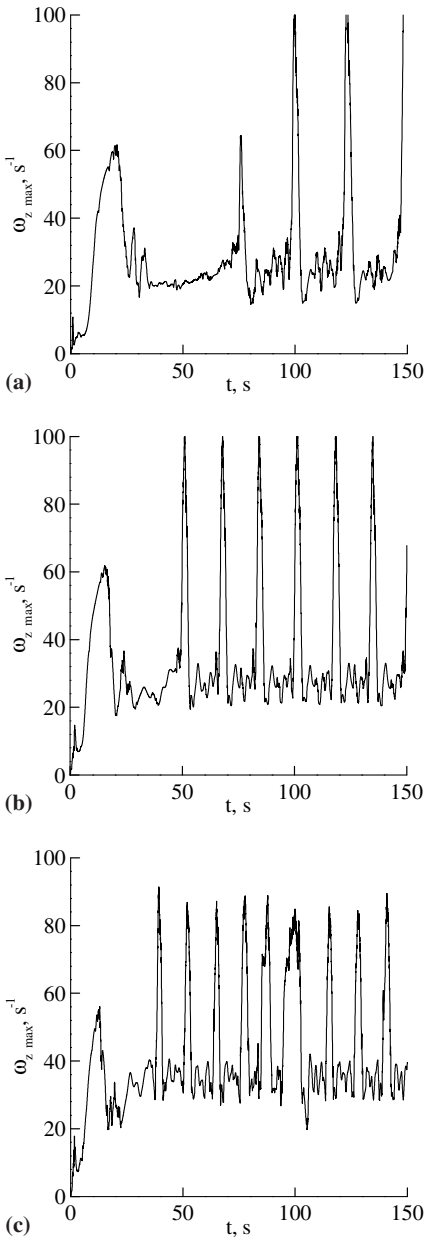

Fig. 11. Periodic formation and destruction of the vortex core. The effect of (constant prescribed) burning rate, $\dot{m}_{fuel}$: (a) 0.010 kg/(m^2 s); (b) 0.020 kg/(m^2 s); (c) 0.040 kg/(m^2 s).

5. Conclusions

Experimental studies of medium (room size) scale whirling fires (missing in the previous research) have been conducted, demonstrating that whirling flames may develop in compartments with ceiling vent and asymmetric air inflow. It has been established that the fire whirls in enclosure are unstable and they exhibit a periodic formation and destruction cycle (of about 10–15 s period for a given experimental arrangement). Flame length and time-averaged mass burning rate in whirling fire were found observably greater than those in non-whirling ones.

To interpret the observed and predicted development of whirling buoyant turbulent diffusion flames, the concepts and results of existing theory of rotating flows have been used. The theory reveals two necessary conditions for buoyant rotating flow to develop: (i) non-zero background vorticity (and external circulation) and (ii) vertical acceleration of the flow. The primary mechanism of vorticity concentration in the vortex core is the stretching of the vortex tube; the latter is balanced by viscous (and possibly turbulent) dissipation. When the above conditions are satisfied, the steady rotating flow has a radial velocity distribution similar to that of the Rankine vortex.

The 3D CFD model and code *Fire3D* earlier developed for predictions of open and enclosed buoyant turbulent diffusion flames have been adapted to simulate whirling fires. The modification to the turbulence model has been introduced to allow for the effect of flow rotation on turbulence. The model has been applied to predict the development of unconfined rotating flames to study the effect of rotation on flame structure, temperature, radiative output. The Rankine-type vortex formation has been demonstrated. Similar to experimental observations, the flame lengthening due to rotation has been predicted. In accordance with the approximate theory, the flame structure and its response on the externally imposed circulation were found to depend on the magnitude of the external circulation and on heat release rate in the flame. The latter determines the length of accelerating part of the flow, where the vorticity is amplified. If the external circulation is imposed then the Rankine-type vortex develops with maximum vorticity (at the axis) and angular velocity (at certain distance away from the axis) proportional to the external circulation. Swirl number of the rotating flow is shown to be proportional to the imposed circulation; at high degree of swirl, flame shortening and destabilisation was predicted.

Local and maximum radiative heat fluxes from the rotating flames (with constant prescribed fuel supply rate) were found to be less then those in non-rotating flames. It can be attributed to change in flame shape (the high temperature radiating flame zone is longer and thinner). It also indicates that additional physical mechanisms should be taken into account to explain and predict the experimentally observed increase in burning rate when the rotation occurs. A possible mechanism, namely entrainment intensification of the air into the fuel rich region near the fuel surface, has been identified.

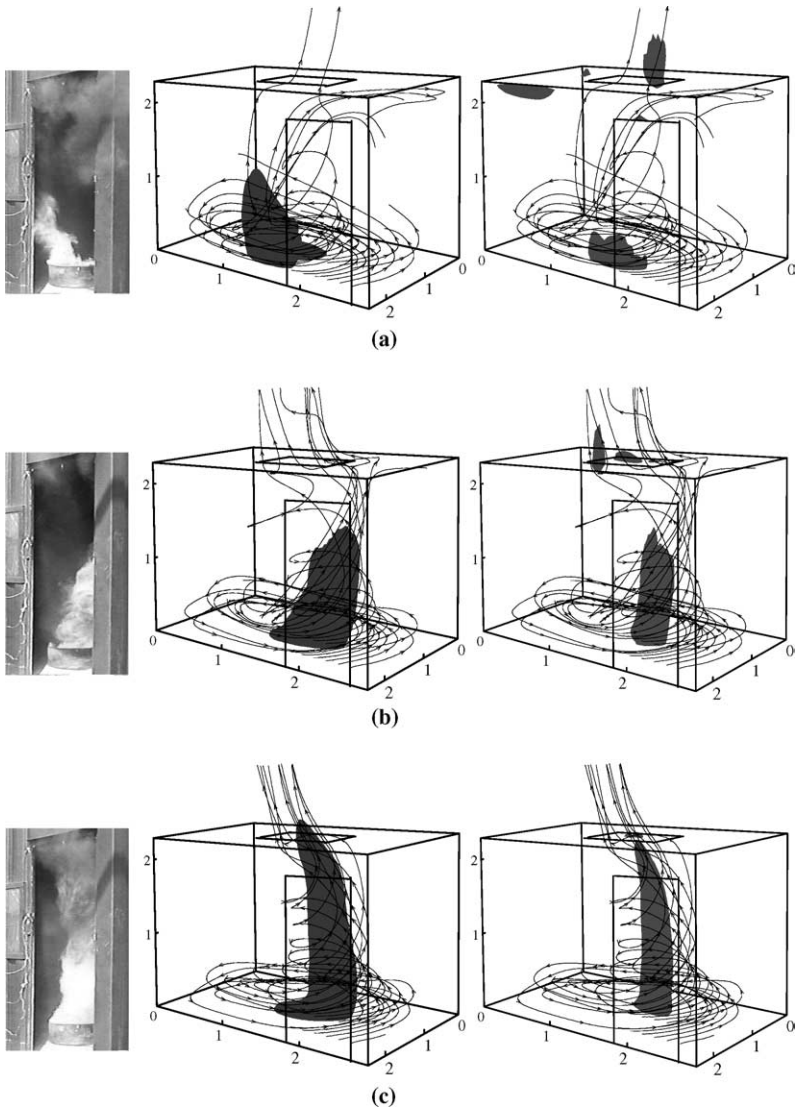

Fig. 12. Comparison of observed and predicted flow. From left to right: frames taken from video; surface $T = 773$ K (approximates visual flame zone); surface $\omega_z = 15\ s^{-1}$ (location of rotating core). Stages of flame development: (a) Flame is deflected towards the rear all, no regular rotation occur. (b) Flame is deflected towards the doorway, whirling zone starts to form. (c) Flame lengthens and straightens, vortex core develops. (d) Flame is straight, it exhausts through the ceiling vent, stretched vortex core erects. (e) Upper part of flame is displaced by rotating incoming airflow, the vortex core travels towards the rear wall. (f) Similar to (a). Streamlines run out from the points at doorway cross-section, at elevations 0.2 and 0.4 m above the floor.

Using *Fire3D*, the whirling flame development was then simulated in the enclosure with the ceiling vent and the asymmetrically located doorway. Circulating air inflow provided the externally imparted vorticity that caused formation of the buoyant whirling flames. The geometry of the enclosure represented that of the experimental compartment. Similar to experimental observations, the predicted whirling fires in enclosure were found to be transient and intrinsically unstable, although of the unconfined flames of the same heat release rate produced steady-state mean flowfields. The periodic process of formation, precession and destruction of the whirling flame was predicted numerically and interpreted in terms of the conclusions from the existing theory of rotating flows.

The period of oscillations was found to decrease if the fuel supply rate increases. It was therefore concluded that more volatile combustibles should cause a higher frequency process. The predicted period is close to that observed in experiments. The flame shape and the

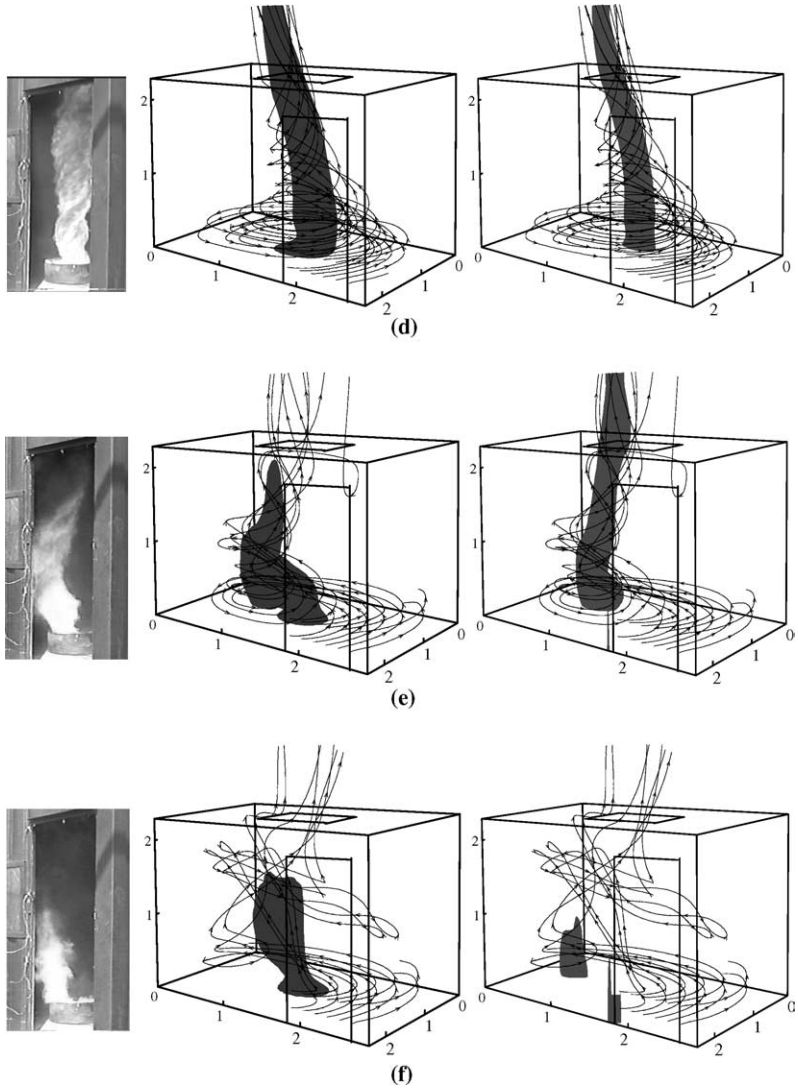

Fig. 12 (*continued*)

flow pattern were compared to those obtained from the video recordings of the experimental flames. The model predictions are in reasonable agreement with the experimental observations of the whirling flame development.

Acknowledgements

The authors thank Mr. Barry Dixon and Mr. John Judd (Greater Manchester County Fire Service) for their support of these studies. This work is a part of research project GR/S69122/01 and RSRG 24350 funded by EPSRC and the Royal Society support from which is gratefully acknowledged.

References

[1] P. Joulain, The behaviour of pool fires: state of the art and new insights, in: Proceedings of the 27th Symposium (Int.) on Combustion. The Combustion Institute, 1998, pp. 2691–2706.

[2] K.S. Mudan, P.A. Croce, Fire hazard calculations for large open hydrocarbon fires, in: SFPE Handbook of Fire Protection Engineering, 2nd ed., NFPA, 1995, pp. 3-197–3-240.

[3] C.L. Beyler, Fire hazard calculations for large, open hydrocarbon fires, in: SFPE Handbook of Fire Protection Engineering, 3rd ed., NFPA, 2002, pp. 3-268–3-314.

[4] A.Yu. Snegirev, Statistical modelling of thermal radiation transfer in buoyant turbulent diffusion flames, Combust. Flame 136 (2004) 51–71.

[5] H.W. Emmons, S.J. Ying, The fire whirl, in: Proceedings of the 11th Symposium (Int.) on Combustion, The Combustion Institute, 1966, pp. 475–488.
[6] A.K. Gupta, D.G. Lilley, N. Syred, Swirl Flows, Abacus Press, 1984.
[7] B.R. Morton, The physics of fire whirls, Fire Res., Abstracts and Reviews 12 (1) (1970) 1–19.
[8] H.J.S. Fernando, D.C. Smith, Vortex structures in geophysical convection, Eur. J. Mech. B: Fluids 20 (2001) 437–470.
[9] S. Soma, K. Saito, Reconstruction of fire whirls using scale models, Combust. Flame 86 (3) (1991) 269–284.
[10] K. Satoh, Numerical study and experiments of fire whirl, in: Proceedings of the 7th International Conference, Interflam'96, 1996, pp. 393–402.
[11] K. Satoh, K.T. Yang, Experimental observations of swirling fires, Proc. ASME, Heat Transfer Division 335 (4) (1996) 393–400.
[12] K. Satoh, K.T. Yang, Simulations of swirling fires controlled by channeled self-generated entrainment flows, in: Proceedings of the 5th Int. Symposium, IAFSS, 1997, pp. 201–212.
[13] K. Satoh, K.T. Yang, Experiments and numerical simulations of swirling fires due to 2×2 flames in a channel with single corner gap, Proc. ASME, Heat Transfer Division 361 (2) (1998) 49–56.
[14] K. Satoh, K.T. Yang, Measurements of fire whirls from a single flame in a vertical square channel with symmetrical corner gaps, Proc. ASME, Heat Transfer Division 364 (4) (1999) 167–173.
[15] N.A. Chigier, J.M. Beer, D. Grecov, K. Bassindale, Jet flames in rotating flow fields, Combust. Flame 14 (1970) 171–180.
[16] J.M. Beer, N.A. Chigier, T.W. Davies, K. Bassindale, Laminarization of turbulent flames in rotating environments, Combust. Flame 16 (1971) 39–45.
[17] J.M. Beer, N.A. Chigier, Combustion Aerodynamics, Wiley, 1972.
[18] D.G. Sloan, P.J. Smith, L.D. Smoot, Modeling of swirl in turbulent flow systems, Progr. Energy Combust. Sci. 12 (1) (1986) 163–250.
[19] S. Imao, M. Itoh, T. Harada, Turbulent characteristics of the flow in an axially rotating pipe, Int. J. Heat Fluid Flow 17 (5) (1996) 444–451.
[20] G.M. Byram, E. Martin, Fire Whirl Winds in the Laboratory, Fire Control Notes 23 (1962) 13–17.
[21] F. Battaglia, R.G. Rehm, H.R. Baum, The fluid mechanics of fire whirls: an inviscid model, Phys. Fluids 12 (11) (2000) 2859–2867.
[22] F. Battaglia, K.B. McGrattan, R.G. Rehm, H.R. Baum, Simulating fire whirls, Combust. Theory Model. 4 (2) (2000) 123–138.
[23] G.K. Batchelor, An Introduction to Fluid Dynamics, Cambridge University Press, 1967.
[24] E.J. Hopfinger, G.J.F. van Heijst, Vortices in rotating fluids, Ann. Rev. Fluid Mech. 25 (1993) 241–289.
[25] A.Yu. Snegirev, G.M. Makhviladze, V.A. Talalov, Statistical modelling of thermal radiation in compartment fire, in: Proceedings of the 9th International Conference Interflam, 2001, vol. 2, pp. 1011–1024.
[26] A.Yu. Snegirev, Monte Carlo modelling of radiative transfer in unconfined buoyant turbulent diffusion flames, Computational thermal radiation in participating media, Proceedings of the Eurotherm Seminar, vol. 73, 2003, pp. 259–270.
[27] G. Cox, Compartment fire modelling, in: G. Cox (Ed.), Combustion Fundamentals of Fire, Academic Press, 1995, pp. 329–404.
[28] M.A. Leschziner, W. Rodi, Calculation of annular and twin parallel jets using various discretization schemes and turbulent-model variations, J. Fluid Eng.: Trans. ASME 103 (1981) 353–360.
[29] W.P. Jones, A. Pascau, Calculation of confined swirling flows with a second moment closure, J. Fluids Eng.: Trans. ASME 111 (1989) 248–255.
[30] K.-C. Chang, C.-S. Chen, Development of a hybrid k–ε turbulence model for swirling recirculating flows under moderate to strong swirl intensities, Int. J. Numer. Meth. Fluids 16 (5) (1993) 421–443.
[31] S.P. Yuan, R.M.C. So, Turbulent rotating flow calculations: an assessment of two-equation anisotropic and Reynolds stress models, Proc. Instn. Mech. Engrs: Part G 212 (1998) 193–212.
[32] D.C. Wilcox, Turbulence Modeling for CFD, DCW Industries, 1998.
[33] G.A. Korn, T.M. Korn, Mathematical Handbook, McGraw-Hill, 1968.